RSC Advances

PAPER

Cite this: *RSC Adv.*, 2019, **9**, 39405

Protein-activated transformation of silver nanoparticles into blue and red-emitting nanoclusters†

Dillip Kumar Sahu, Priyanka Sarkar, Debabrata Singha and Kalyanasis Sahu *

Received 27th August 2019
Accepted 23rd November 2019

DOI: 10.1039/c9ra06774d

rsc.li/rsc-advances

Proteins are very effective capping agents to synthesize biocompatible metal nanomaterials *in situ*. Reduction of metal salts in the presence of a protein generates very different types of nanomaterials (nanoparticles or nanoclusters) at different pH. Can a simple pH jump trigger a transformation between the nanomaterials? This has been realized through the conversion of silver nanoparticles (AgNPs) into highly fluorescent silver nanoclusters (AgNCs) *via* a pH-induced activation with bovine serum albumin (BSA) capping. The BSA-capped AgNPs, stable at neutral pH, undergo rapid dissolution upon a pH jump to 11.5, followed by the generation of blue-emitting Ag_8NCs under prolonged incubation (~9 days). The AgNPs can be transformed quickly (within 1 hour) into red-emitting Ag_{13}NCs by adding sodium borohydride during the dissolution period. The BSA-capping exerts both oxidizing and reducing properties in the basic solution; it first oxidizes AgNPs into Ag^+ and then reduces the Ag^+ ions into AgNCs.

Noble metal nanomaterials, especially silver (Ag) and gold (Au), have witnessed exceptional research exploration in the last couple of decades from both fundamental and application perspectives.[1] These nanomaterials mainly exist in two distinct size regimes with unique optical characteristics. Ultra-small nanoclusters (NCs) (size typically <3 nm) contain only a handful of atoms (few to hundred), while relatively large nanoparticles (NPs) may comprise thousands of atoms. NPs may display strong extinction (absorption or scattering) spectra in the UV-vis region but are generally non-fluorescent.[2] In contrast, metal nanoclusters (MNCs) exhibit bright emission but not so noteworthy absorption spectra.[3,4] The distinct optical characteristics of the two nanomaterials have been exploited in various applications. For example, metal nanoparticles (MNPs) are extensively used in photothermal therapy[5] and imaging,[6] while NCs are more suited in fluorescence imagining[7] and sensing[8] applications. A facile transformation between the two nanomaterials could enable us to combine the complementary optical properties in a single system. Moreover, the kinetics of transformation can provide insights on various intermediate processes like dissolution, etching and digestive ripening *etc.*[9–11]

Silver nanoparticles (AgNPs) and nanoclusters (AgNCs) are of particular interest, as it not only possess the intriguing physicochemical properties of MNPs and MNCs, but also feature unique properties pertaining to silver.[3,12,13] For example, metallic silver has been well known for its capability to prevent infection since the ancient times, while recent studies revealed that ultrasmall AgNCs exhibit even superior antibacterial properties towards a broad spectrum of bacteria.[13,14] Moreover, due to superior plasmonic properties and bright fluorescence, AgNPs and AgNCs are preferred over other metal nanomaterials.[15,16]

The fluorescence properties of AgNCs mainly be attributed to the quantum confinement effect or surface ligand effect.[17] The strong fluorescence generally arises from the electronic transition between occupied d band and states above the Fermi level (sp bands) or the electronic transition between highest occupied molecular orbital (HOMO) and the lowest unoccupied molecular orbital (LUMO).[18] Several reviews have been devoted for the fundamental understanding of the fluorescence origin of AgNCs.[17,19] Recently, it was demonstrated that aggregation-induced emission (AIE) may also contribute to the luminescence pathway of MNCs.[19,20] The origin of AIE from MNCs could be attributed to the restriction of intramolecular vibration and rotation of ligand on the surface of MNCs after aggregation, which facilitates the radiative energy relaxation *via* inhibiting of non-radiative relaxations.[21,22]

Protein capping is quite common for obtaining both NPs[23,24] and NCs.[25–29] Serum proteins, bovine serum albumin (BSA) and human serum albumin (HSA) are the most popular among trials with different proteins.[26–29] BSA is a large protein which provides steric stabilization to the MNCs with its various functional group like –OH, $–NH_2$, –COOH, –SH.[25,30] The disulfide

Department of Chemistry, Indian Institute of Technology Guwahati, Guwahati 781039, India. E-mail: ksahu@iitg.ac.in

† Electronic supplementary information (ESI) available: Experimental section; stability of AgNPs-BSA; TEM image after NaOH treatment; excitation spectra of AgNCs; effect of $NaBH_4$ on dissolution of AgNPs; fluorescence decays and fit parameters of AgNCs; emission spectra of red AgNCs at low temperature and at low pH and dissolution kinetics of AgNP. See DOI: 10.1039/c9ra06774d

bond of BSA may have strong interaction with the MNCs where sulfur may be covalently bonded to the MNCs core.[24,31] The nanomaterials are synthesized within the protein template at very different pHs. AgNPs are obtained from the reduction of silver salts at neutral pH (6–8),[24] whereas the same process at a higher pH (>11) leads to AgNCs.[30,32] The protein capping itself may reduce Ag^+; AgNCs are formed without any external reducing agent.[25,33] However, an external reducing agent may change the nature and kinetics of the NCs significantly.[30]

Thus, the influence of pH on the protein structure may govern the selective synthesis of AgNPs or AgNCs. BSA can achieve several conformations – N (native), B (basic), A (aged) and U (unfolded) as the pH of the medium gradually changes from neutral to highly alkaline.[34,35] It may be possible that a specific type of nanomaterial is stable within a particular conformation dictated by the pH of the medium. Hence, by simply changing the pH, we may expect a significant modulation of the morphology of the nanomaterial. Herein, we applied this concept to show an effortless transformation from AgNP to AgNC. Although BSA template is exceptionally popular in the preparation of both AgNPs and AgNCs, however, to the best of our knowledge, no report is available on the conversion from AgNP to AgNC within the protein capping.

The BSA-capped AgNPs (BSA-AgNPs) were first synthesized at a neutral pH (pH = 6) using sodium borohydride reduction (see ESI†). The AgNPs show a sharp surface plasmon resonance (SPR) band at 415 nm (Fig. 1a) and have uniform diameters of 12.5 ± 1.5 nm (Fig. 1b). The AgNPs are quite stable at this pH with no apparent change in the SPR band even after 15 days (Fig. S1†).

However, when the BSA-AgNPs were treated with NaOH to elevate the pH to 11.5, we observed a remarkable decrease in the SPR band at 415 nm and a color change from dark to light brown within 2 h of the pH jump (Fig. 2a). The observations indicate the dissolution of AgNPs, which was further confirmed from the TEM images taken quickly (~10 min) after the NaOH treatment (Fig. S2†). Heterogeneous distribution of AgNPs was obtained with sizes varying from 2.6 nm to 17 nm, which is in sharp contrast to the uniform AgNPs before the addition NaOH (*cf.* Fig. 1b). Upon further incubation (6 h), the light brown color gradually faded to light yellow with a further decrease in the SPR band absorbance (Fig. S3†).

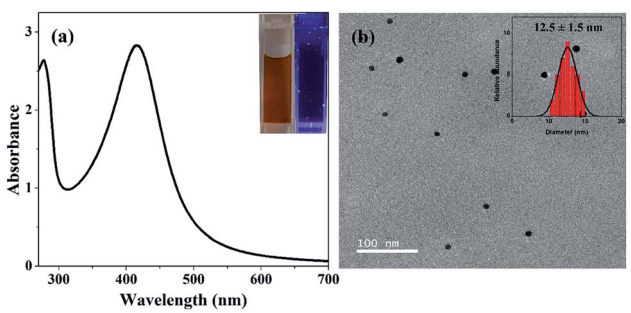

Fig. 1 (a) UV-vis spectrum and (b) TEM image of BSA-protected AgNPs synthesized at pH 6. The insets show the appearance of the AgNP solution under regular and UV light (left panel), and size distribution histogram (right panel).

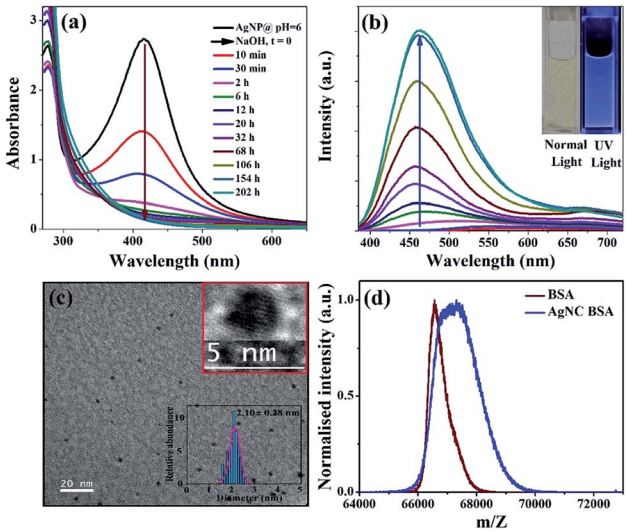

Fig. 2 Time evaluation of the (a) UV-visible and (b) emission spectra (λ_{ex} = 370 nm) of BSA-capped AgNPs after enhancement of the pH from 6 to 11.5 (by addition of NaOH at t = 0). The inset shows the snapshot of the final blue-emitting AgNC solution under normal and UV lights. (c) TEM of the blue-emitting AgNCs along with the HRTEM image and the analyzed size distribution in the inset. (d) MALDI-mass spectra of the BSA protein and BSA-capped blue-emitting AgNCs.

Interestingly, the solution also develops distinct fluorescence with a maximum at ~460 nm after the addition of NaOH (Fig. 2b). The fluorescence intensity gradually grows up upon incubation, and finally, an intense blue fluorescence was developed within ~9 days. The final NaOH-treated AgNP solution appears to be light yellow under normal light and blue-fluorescent when viewed under a hand-held UV lamp (Fig. 2b, inset). The blue-emitting AgNCs exhibit a single band excitation spectrum with a maximum at 372 nm (Fig. S4†).

TEM image of the optimized NCs (after 9 days incubation at 37 °C) exclusively reveals uniform AgNCs of ~2.10 ± 0.28 nm diameter without any trace of large NPs (Fig. 2c). The mass of the BSA-capped AgNCs (67 375 Da) was shifted by 845 Da from that of native BSA (66 530 Da) (Fig. 2d). Thus, the new species should correspond to Ag_8 cluster. The characteristics of the blue-AgNCs were quite similar to the human serum albumin (HSA)-protected blue-AgNCs, directly prepared from silver salt.[33] However, the formation time of those AgNCs was significantly less (~10 h) than the present method (~9 days).[33] Thus, the initial dissolution process, although quite fast, may have a crucial role in the kinetics of the protein-protected NCs. When we performed a similar pH jump experiment on a citrate-stabilized AgNP,[36] the extinction spectrum of the AgNPs showed much less variation compared to the BSA-AgNPs. Instead of a strong decrease, the SRP band showed a red-shift with an extended tail indicating aggregation rather than dissolution of NPs (Fig. S5†).

Furthermore, a red-emitting cluster was generated when an external reducing agent, sodium borohydride ($NaBH_4$), was added during the dissolution process. $NaBH_4$ was added after ~11 min of the NaOH addition when the SPR band of BSA-AgNP

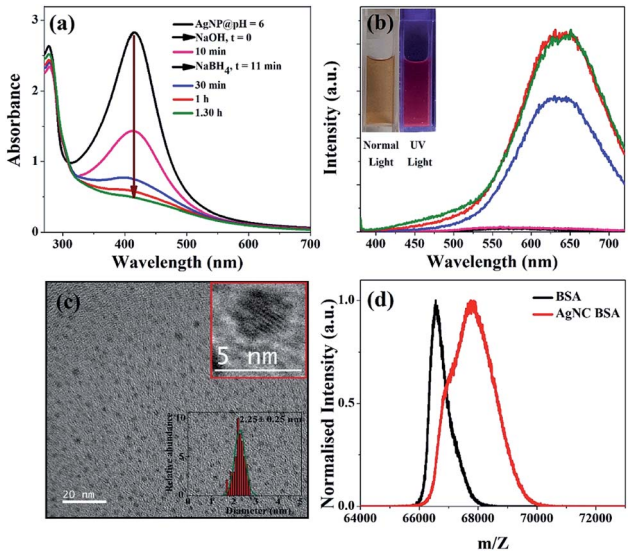

Fig. 3 Early time evolution of (a) UV-visible and (b) emission spectra (λ_{ex} = 370 nm) of the BSA-protected AgNPs upon subsequent treatments with NaOH (pH 11.5) and $NaBH_4$ at t = 0 and 11 min, respectively. The decrease of the SPR band at 415 nm and a concomitant increase of the fluorescence band at ~650 nm indicates dissolution of the AgNPs and formation of the red-emitting cluster. The inset shows the visuals of the AgNCs formed after 1 h under normal light and UV light. (c) TEM of the red-emitting AgNCs along with the HRTEM image and the analyzed size distribution in the inset. (d) MALDI-mass spectra of the BSA protein and BSA-capped red-emitting AgNCs.

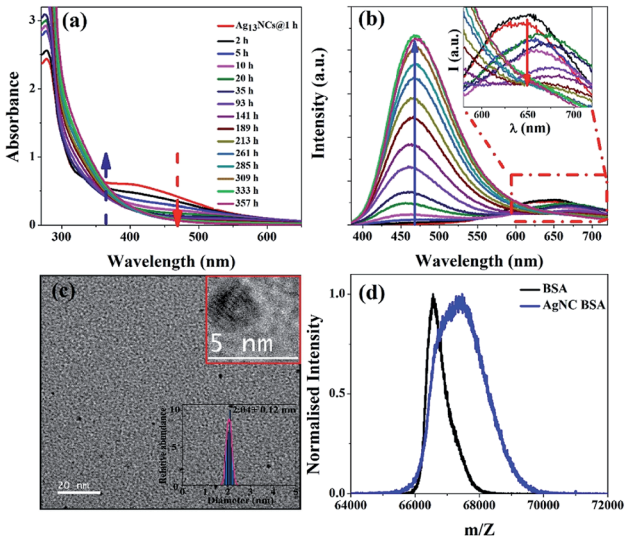

Fig. 4 Transformation of red-emitting to blue-emitting cluster: (a) UV-visible and (b) emission spectra (λ_{ex} = 370 nm) showing transformation of the BSA-protected red-emitting Ag_{13}NCs (obtained at 1 h) to blue-emitting AgNC upon prolonged incubation. Red and blue arrows respectively denote the decrease/increase of the red/blue cluster absorbance and emission intensity with time. The inset (b) shows a magnified wavelength region in 580–720 nm of the emission spectra. (c) TEM image of the blue-emitting silver nanocluster while its inset shows HRTEM image with size histogram of corresponding silver nanocluster. (d) MALDI-mass spectra of BSA and BSA-containing blue-emitting silver nanocluster synthesized from Ag_{13}NCs.

was already decreased by half (Fig. 3a). The SPR band (λ_{max} = 415 nm) of AgNP continues to diminish similarly before and after the addition of $NaBH_4$ (Fig. S3†). Thus, $NaBH_4$ may not have any significant effect on the dissolution process of AgNP. However, it has a strong impact on the modulation of the fluorescence; a new fluorescence band was developed at ~650 nm within a much shorter duration (1 h) (Fig. 3b). The solution exhibits a bright-red fluorescence under a UV lamp (Fig. 3b, inset) with a quantum yield of 3.5%.

TEM measurements of the red-emitting species show homogeneous distribution of AgNCs with ~2.25 ± 0.25 nm diameter (Fig. 3c). MALDI-mass experiment further assigned the red-emitting species as Ag_{13} cluster (Fig. 3d). The excitation spectrum (λ_{em} = 650 nm) displays two distinct peaks at 370 nm and 470 nm, which match closely to the reported excitation peaks of the Ag_{13-15} clusters within BSA/HSA capping (Fig. S4†).[30,32,33] Moreover, the fluorescence decay of the red-emitting-AgNCs converted from AgNP almost matches with those prepared directly from $AgNO_3$; both display very similar average lifetimes (0.95 ns *vs.* 0.89 ns) (Fig. S6 and Table S1†).[37]

Another important observation is that the red-emitting AgNCs have only transient stability at 37 °C. With further incubation, the absorbance at ~470 nm (characteristic excitation peak of the red-emitting cluster) reduces and the absorbance at 370 nm (excitation peak of the blue-emitting cluster) increases simultaneously (Fig. 4a). The red-emission at 650 nm also decreases gradually with a concomitant increase of a blue emission band at 465 nm (Fig. 4b). Thus, both absorption and emission measurements clearly indicate transformation of red- to blue-emitting clusters which takes up to ~15 days for completion. The solution finally becomes light yellow and exhibits a bright blue fluorescence under UV light similar to the blue-emitting cluster obtained earlier from the AgNP in the absence of $NaBH_4$. Interestingly, other characteristics of the regenerated blue-emitting AgNCs (converted from Ag_{13}NCs) also match quite nicely with the directly prepared blue-AgNCs (converted from AgNPs in the absence of $NaBH_4$). The size of this blue cluster was 2.04 ± 0.12 nm, which is similar to the previously obtained direct blue-emitting cluster (2.10 ± 0.28) (Fig. 4c). Furthermore, MALDI-mass measurement reveals that both the blue-emitting clusters may have the same composition, Ag_8 (Fig. 4d). In addition to this, the average lifetime (0.53 ns) of the blue-emitting AgNCs synthesized from AgNP agrees well to the average lifetime (0.40 ns) of the blue-emitting AgNCs converted from the red-emitting AgNCs (Fig. S7 and Table S2†). However, the quantum yield (23%) of blue-emitting AgNCs, converted from red-emitting AgNCs, was higher than the quantum yield (18%) of the blue-emitting AgNCs, converted from AgNPs. Since, the emission characteristics of the blue and the red-emitting clusters nearly matches with earlier report, we expect that silver may be present in the zero oxidation state as determined in those studies.[30,31]

Moreover, the atomic composition of the NCs can be also be estimated from the Jellium model using the equation[38,39]

$$E_{em} = E_{Fermi}/N^{0.33}$$

where E_{Fermi} is the Fermi energy of the metal (Ag), E_{em} is the emission energy of the MNCs and N is the number of atoms constituting a MNC. Using the model equation, the number of silver atoms for the blue-emitting AgNCs can be predicted as 8.45 (~8) Ag atoms which is a good agreement with our MALDI data (8 Ag atoms). However, the theoretical calculation estimated as $N \sim 24$ for the red-emitting AgNCs, which is not in agreement with the MALDI data (13 Ag atoms). This is because of the well-known deviation of the Jellium model for higher number of Ag atoms in AgNCs because of increase in the electronic screening effects and the harmonic distortion in the potential energy well.[19]

Although the red-emitting cluster is not very stable at the experimental condition (pH 11.5, 37 °C), it may be easily stabilized by lowering the temperature or pH. The fluorescence intensity of the red-emitting and blue-emitting cluster kept at 4 °C, was almost preserved for more than 15 days (Fig. S8†). On the other hand, lowering the pH to 6, also inhibits the red to blue-cluster transformation (Fig. S9†). The observations indicate that the red-blue transformation has a moderate activation barrier and the conversion may be governed by the change in the structure of the protein in the alkaline condition. Acidification of the solution can stop the transformation of the protein conformation and inhibits the process.

From these observations, we may conclude that the conversion from NPs to NCs occurs in two steps. First, a rapid dissolution of AgNP occurs in the alkaline medium. The kinetics of the dissolution process can be monitored through a time-dependent decrease of the SPR band and the time constant was found to be ~13 min (Fig. S10†). Dissolution of AgNPs is an important issue and assumed to be the leading cause of toxicity of AgNPs in biological mediums.[40] The dissolution is commonly favored at a low pH but drastically inhibited at high pH.[41] The swift dissolution of the BSA-protected AgNP observed here at a high pH (11.5) is unprecedented. Thus, the BSA capping may have an active role in the dissolution process. We comprehend that the oxidation power of protein may be activated in the basic medium.

Organothiols (R-SH) are known to promote dissolution of AgNPs; R-SH progressively reacts with Ag atoms to form RS-Ag complex.[42] Since cysteine is also an organothiol, it is expected to play an essential role in the dissolution of AgNPs. Gondikas *et al.* showed that excess cysteine could favor the dissolution process of AgNPs, whereas another amino acid, serine (S–H bond is replaced by O–H bond), has no effect.[43] Zang and coworkers showed that only the isolated or reduced cysteine in a protein has a dominant role in the dissolution of NPs.[44] Although BSA contains as many as 35 cysteine residues; 34 of them are involved in S–S bond formation and only a single cysteine is present in free form (S–H). Hence, the dissolution of AgNPs at neutral pH may be negligible.

Most proteins rich in sulfur-containing residues (cysteine and methionine) may degrade in alkaline solution. Florence reported that about 5 of 17 S–S bridges in BSA may be cleaved in the presence of 0.2 M NaOH.[45] Thus, at higher pH, some disulfide bonds may be cleaved and more cysteine residues may participate in the dissolution of BSA-capped AgNPs.

In the second step, Ag^+ ions generated from the dissolution of AgNPs, can be reduced either by the protein capping itself or by an external reducing agent to form NCs (Scheme 1). The tyrosine residues may be responsible for the reduction of the metal ions to NCs.[25,33] At a pH, higher than the pKa (10.46) of tyrosine, the reduction capability of tyrosine is enhanced by deprotonation of the phenolic group.[25,33,46] Moreover, the addition of a strong reducing agent (*e.g.*, $NaBH_4$) may lead to a faster reduction, which favors quicker nucleation and growth of Ag atoms forming the bigger NCs (Ag_{13}NCs). However, the large Ag_{13}NCs may not be adequately stabilized by the protein conformation at that condition and hence may transform into the more stable blue-emitting Ag_8NCs.

The conformation change of the protein capping during the conversion was also supported by the circular dichroism (CD) measurements (Fig. S11†). The formation of AgNPs results in a negligible change in the protein conformation (Table S3†). However, the formation of red Ag_{13} cluster results in a substantial modification in the BSA conformation. The α helix content reduces from 57% to 49%, whereas coil randomness increases from 17% to 21% without a major change in the β sheet. Interestingly, blue-emitting Ag_8 cluster perturbed the conformation of the BSA to a much larger extent (Table S3†). As the cysteine disulfide bond has a direct role on maintaining the folded conformation of BSA, its breaking may change the protein conformation. The addition of NaOH induces breaking of S–S bond, which leads to formation of AgNCs with subsequent change in protein secondary structure.

In conclusion, we report an unprecedented fast dissolution of AgNPs through activation of the protein (BSA) capping by elevating the pH of the medium to 11.5. At higher pH, the disulfide bonds may be cleaved, and the free cysteine may activate the dissolution process. The protein capping also plays a crucial role in the formation of fluorescent nanocluster after the completion of the dissolution process. Thus, we explored multiple roles of the BSA capping – (1) a stable capping agent at neutral pH to stabilize the AgNPs (2) activates the dissolution process probably *via* oxidative dissolution of the AgNPs (3) adsorbing the nascent silver ions within its scaffold and (4) finally reducing them to fluorescent nanocluster.

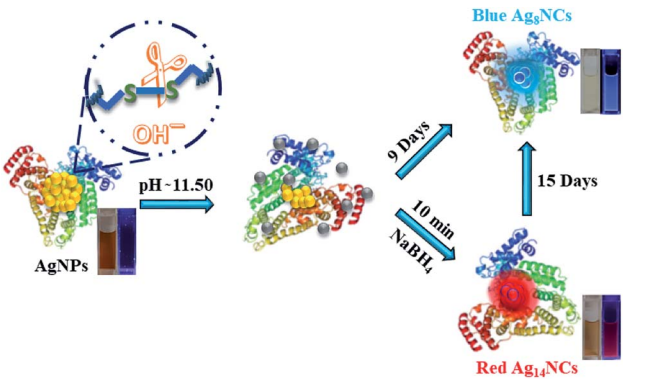

Scheme 1 Schematic representation of the transformation of the BSA-capped AgNPs to blue- and red-emitting AgNCs.

Conflicts of interest

There are no conflicts to declare.

Acknowledgements

The work is funded by the Department of Science and Technology (DST), India (EMR/2014/000011). We thank the Department of Chemistry and Central Instrument Facility for the instrument facility. DKS and PS thank the Indian Institute of Technology Guwahati for fellowships.

Notes and references

1 P. K. Jain, X. Huang, I. H. El-Sayed and M. A. El-Sayed, *Acc. Chem. Res.*, 2008, **41**, 1578–1586.
2 S. Link and M. A. El-Sayed, *J. Phys. Chem. B*, 1999, **103**, 8410–8426.
3 I. Díez and R. H. A. Ras, *Nanoscale*, 2011, **3**, 1963–1970.
4 J. Zheng, P. R. Nicovich and R. M. Dickson, *Annu. Rev. Phys. Chem.*, 2007, **58**, 409–431.
5 S. C. Boca, M. Potara, A.-M. Gabudean, A. Juhem, P. L. Baldeck and S. Astilean, *Cancer Lett.*, 2011, **311**, 131–140.
6 D. Boyer, P. Tamarat, A. Maali, B. Lounis and M. Orrit, *Science*, 2002, **297**, 1160–1163.
7 Z. Luo, K. Zheng and J. Xie, *Chem. Commun.*, 2014, **50**, 5143–5155.
8 S. Ghosh, U. Anand and S. Mukherjee, *Anal. Chem.*, 2014, **86**, 3188–3194.
9 L. Dhanalakshmi, T. Udayabhaskararao and T. Pradeep, *Chem. Commun.*, 2012, **48**, 859–861.
10 H.-H. Deng, K.-L. Li, Q.-Q. Zhuang, H.-P. Peng, Q.-Q. Zhuang, A.-L. Liu, X.-H. Xia and W. Chen, *Nanoscale*, 2018, **10**, 6467–6473.
11 D. Bain, B. Paramanik and A. Patra, *J. Phys. Chem. C*, 2017, **121**, 4608–4617.
12 H. Xu and K. S. Suslick, *Adv. Mater.*, 2010, **22**, 1078–1082.
13 K. Zheng, X. Yuan, N. Goswami, Q. Zhang and J. Xie, *RSC Adv.*, 2014, **4**, 60581–60596.
14 X. Yuan, M. I. Setyawati, D. T. Leong and J. Xie, *Nano Res.*, 2014, **7**, 301–307.
15 D. Singha, N. Barman and K. Sahu, *J. Colloid Interface Sci.*, 2014, **413**, 37–42.
16 R. Jin, C. Zeng, M. Zhou and Y. Chen, *Chem. Rev.*, 2016, **116**, 10346–10413.
17 L. Zhang and E. Wang, *Nano Today*, 2014, **9**, 132–157.
18 S. Link, A. Beeby, S. FitzGerald, M. A. El-Sayed, T. G. Schaaff and R. L. Whetten, *J. Phys. Chem. B*, 2002, **106**, 3410–3415.
19 N. Goswami, Q. Yao, Z. Luo, J. Li, T. Chen and J. Xie, *J. Phys. Chem. Lett.*, 2016, **7**, 962–975.
20 H. Zhang, Z. Zhao, P. R. McGonigal, R. Ye, S. Liu, J. W. Y. Lam, R. T. K. Kwok, W. Z. Yuan, J. Xie, A. L. Rogach and B. Z. Tang, *Mater. Today*, 2019, DOI: 10.1016/j.mattod.2019.08.010.
21 J. Mei, N. L. C. Leung, R. T. K. Kwok, J. W. Y. Lam and B. Z. Tang, *Chem. Rev.*, 2015, **115**, 11718–11940.
22 J. Wang, X. Lin, T. Shu, L. Su, F. Liang and X. Zhang, *Int. J. Mol. Sci.*, 2019, **20**, 1891.
23 P. Murawala, S. M. Phadnis, R. R. Bhonde and B. L. V. Prasad, *Colloids Surf., B*, 2009, **73**, 224–228.
24 A. Gebregeorgis, C. Bhan, O. Wilson and D. Raghavan, *J. Colloid Interface Sci.*, 2013, **389**, 31–41.
25 J. Xie, Y. Zheng and J. Y. Ying, *J. Am. Chem. Soc.*, 2009, **131**, 888–889.
26 S. S. Narayanan and S. K. Pal, *J. Phys. Chem. C*, 2008, **112**, 4874–4879.
27 X. L. Guével, N. Daum and M. Schneider, *Nanotechnology*, 2011, **22**, 275103.
28 H. Wei, Z. Wang, L. Yang, S. Tian, C. Hou and Y. Lu, *Analyst*, 2010, **135**, 1406–1410.
29 A. Aires, I. Llarena, M. Moller, J. Castro-Smirnov, J. Cabanillas-Gonzalez and A. L. Cortajarena, *Angew. Chem., Int. Ed.*, 2019, **58**, 6214–6219.
30 A. Mathew, P. R. Sajanlal and T. Pradeep, *J. Mater. Chem.*, 2011, **21**, 11205–11212.
31 X. Le Guével, B. Hötzer, G. Jung, K. Hollemeyer, V. Trouillet and M. Schneider, *J. Phys. Chem. C*, 2011, **115**, 10955–10963.
32 A. S. Patel and T. Mohanty, *J. Mater. Sci.*, 2014, **49**, 2136–2143.
33 U. Anand, S. Ghosh and S. Mukherjee, *J. Phys. Chem. Lett.*, 2012, **3**, 3605–3609.
34 P. Sen, B. Ahmad and R. H. Khan, *Eur. Biophys. J.*, 2008, **37**, 1303.
35 A. Basir, K. Mohammad Zahid and K. Rizwan Hasan, *Protein Pept. Lett.*, 2004, **11**, 307–315.
36 L.-Q. Zheng, X.-D. Yu, J.-J. Xu and H.-Y. Chen, *Talanta*, 2014, **118**, 90–95.
37 D. K. Sahu, T. Pal and K. Sahu, *ChemPhysChem*, 2018, **19**, 2153–2158.
38 J. Zheng, C. Zhang and R. M. Dickson, *Phys. Rev. Lett.*, 2004, **93**, 077402.
39 N. K. Das, S. Ghosh, A. Priya, S. Datta and S. Mukherjee, *J. Phys. Chem. C*, 2015, **119**, 24657–24664.
40 J. Liu, D. A. Sonshine, S. Shervani and R. H. Hurt, *ACS Nano*, 2010, **4**, 6903–6913.
41 B. Molleman and T. Hiemstra, *Environ. Sci.: Nano*, 2017, **4**, 1314–1327.
42 S. M. Ansar, G. S. Perera, P. Gomez, G. Salomon, E. S. Vasquez, I. W. Chu, S. Zou, C. U. Pittman, K. B. Walters and D. Zhang, *J. Phys. Chem. C*, 2013, **117**, 27146–27154.
43 A. P. Gondikas, A. Morris, B. C. Reinsch, S. M. Marinakos, G. V. Lowry and H. Hsu-Kim, *Environ. Sci. Technol.*, 2012, **46**, 7037–7045.
44 K. Siriwardana, A. Wang, M. Gadogbe, W. E. Collier, N. C. Fitzkee and D. Zhang, *J. Phys. Chem. C*, 2015, **119**, 2910–2916.
45 T. M. Florence, *Biochem. J.*, 1980, **189**, 507–520.
46 J. Xie, J. Y. Lee, D. I. C. Wang and Y. P. Ting, *ACS Nano*, 2007, **1**, 429–439.